

# Metabolomic analysis and pharmacological validation of the cerebral protective effect of 3,4-dihydroxybenzaldehyde on cerebral ischemia-reperfusion injury

YUAN LUO, PU CHEN, LIPING YANG and XIAOHUA DUAN

Yunnan Key Laboratory of Dai and Yi Medicine, Yunnan University of Chinese Medicine, Kunming, Yunnan 650500, P.R. China

Received August 12, 2022; Accepted October 28, 2022

DOI: 10.3892/mmr.2022.12896

**Abstract.** 3,4-Dihydroxybenzaldehyde (DBD), one of the active components of *Gastrodia elata*, has a cerebral protective effect and can effectively combat cerebral ischemia/reperfusion (I/R) injury in rats. However, the metabolite profiles and underlying mechanisms associated with DBD remain unclear. To explore the level of energy metabolism and pharmacological targets in brain tissue following DBD treatment of stroke. The right middle cerebral artery of the rats was occluded for 2 h and reperfused for 24 h to simulate brain I/R injury. Pharmacological results showed that DBD reduced cerebral infarct volume, improved neurological function and increased adenosine triphosphate (ATP) content. Mitochondria are the primary sites for ATP generation and cellular energy supply and decreasing mitochondrial dysfunction can alleviate the energy expenditure of ischemic stroke. Through further experiments, it was found that mitochondrial damage was recovered following DBD treatment, which was manifested by the improvement of mitochondrial morphology under an electron microscope and the reduction of oxidative stress damage. The metabolomics of middle cerebral artery occlusion/reperfusion (MCAO/R) rat brain tissue was studied by the liquid chromatography-tandem mass spectrometry metabolomics method. Significantly different metabolites were screened and the pathways involved included amino sugar and nucleotide sugar metabolism and pentose phosphate pathway. Finally, the present study performed targeted metabolic profiling and validated potential therapeutic targets. Uridine diphosphate N-acetylglucosamine (UDP-GlcNAc) levels were decreased in the MCAO/R group

but significantly increased in the DBD group. TdT-mediated dUTP nick end labeling (TUNEL) staining, hematoxylin and eosin staining and western blotting showed that brain cell apoptosis was inhibited and neuronal morphology improved. Among them, the regulatory enzyme O-GlcNAc transferase (OGT) of UDP-GlcNAc appeared to be significantly increased and neuronal apoptosis was inhibited following DBD treatment, which was verified by western blotting. Therefore, by analyzing mitochondrial dysfunction following I/R and the characterization of potential markers in mitochondrial energy metabolism, it was shown that OGT could inhibit neuronal apoptosis as a potential therapeutic target for brain I/R injury.

## Introduction

Ischemic stroke (IS) is one of the most common disorders and accounts for ~ 80% of strokes. Stroke is the second leading cause of morbidity (158/100,000/year) (1) and mortality (11.6% of total deaths) (2) worldwide after cardiovascular diseases (3). In general, early blood supply or reperfusion is the most effective method for treating cerebral ischemia; however, reperfusion after ischemia can result in severe brain failure, known as cerebral ischemia/reperfusion (I/R) injury (4,5). Studies suggest that mitochondria are severely damaged in I/R injury (6,7). In addition, abnormal oxygen supply can inactivate the initiation of the tricarboxylic acid (TCA) cycle and subsequently inhibit mitochondrial oxidative phosphorylation; this can lead to adenosine triphosphate (ATP) deficiency, thus inducing mitochondrial dysfunction. Including oxygen-free radical damage, calcium overload and changes in mitochondrial membrane potential (MMP), the abnormal opening of the mitochondrial permeability transition pore (mPTP) and mitochondrial structural damage (8,9) can directly lead to neuronal necrosis and loss of brain function (10). Therefore, the relationship between stroke and mitochondria has been actively explored and neuroprotection is considered a promising stroke treatment strategy (11). More effective neuroprotective measures and drugs for the clinical prevention and treatment of cerebral I/R injury based on the mitochondrial pathway are required.

Chinese herbal medicine has long been used in the treatment of stroke. Its rich drug resources and long-term

---

*Correspondence to:* Dr Xiaohua Duan, Yunnan Key Laboratory of Dai and Yi Medicine, Yunnan University of Chinese Medicine, 1076 Yuhua Road, Chenggong, Kunming, Yunnan 650500, P.R. China  
E-mail: 1047896527@qq.com

**Key words:** ischemic stroke, 3,4-dihydroxybenzaldehyde, metabolomics, mitochondrial dysfunction, uridine diphosphate N-acetylglucosamine, O-GlcNAc transferase

treatment experience indicate its great application potential for stroke treatment (12). Notably, *Gastrodia elata* Blume has been used as an anticonvulsant in eastern countries for several centuries. Clinically, it has been widely used to treat headache, epilepsy, limb numbness, hemiplegia and other neurological diseases disorders (13); it has also been approved by the Chinese Pharmacopoeia (14). A phenolic component of *G. elata*, 3,4-dihydroxybenzaldehyde (DBD; Fig. 1A), exhibits neuroprotective effects for cerebral I/R injury after IS (15,16). Our previous study reported that DBD can inhibit the activation of MAPK and NF- $\kappa$ B, reduce the secretion of inflammatory mediators and cytokines and exhibit antineuritis effects (17). In addition, the ethyl acetate site of *G. elata* where DBD is located can enhance the expression of tight junction proteins and protect the blood-brain barrier (BBB) (18,19). For middle cerebral artery occlusion/reperfusion (MCAO/R) rats, neuroprotective effects are observed by creating anti-oxidative stress and inhibiting apoptotic pathways (15,20). Recently, Zeng *et al* (21) indicated that DBD could inhibit the hypoxia-inducible factor-1  $\alpha$ /pyruvate dehydrogenase kinase 1 signaling pathway, alleviate mitochondrial metabolic disorder in the internal capsule after brain I/R and improve energy deficiency *in vitro* and *in vivo*. These aforementioned studies indicate that DBD may play an anti-IS role in the brain. However, previous experiments have not comprehensively explored the relevant mechanism of DBD in stroke treatment from the metabolite level; thus, further research is needed.

Metabolomics is a powerful research method in the field of systems biology. Gene functions and metabolic pathways associated with phenotypes can be detected by identifying a range of genes and metabolites (22). In addition, disease-specific metabolites can be used as biomarkers for the diagnosis of diseases, thus providing a reference for clinical precision medicine (23). Mechanistic studies on traditional Chinese medicine (TCM) pharmacology combined with metabolomics may help understand the complete metabolic network and be used as an effective method for identifying the multiple interactions among TCM components (24). Accordingly, the present study combined metabolomics and pharmacology to investigate the neuroprotective effects of DBD systematically and scientifically on brain I/R injury. Liquid chromatography-tandem mass spectrometry (LC-MS) has become the mainstream of metabolomic research because of its analysis speed, high resolution and high sensitivity (25). Therefore, the present study aimed to use the LC-MS/MS metabolomics approach to study the brain tissue metabolome of MCAO/R rats and explore the intervention mechanism of DBD through energy metabolomic analysis combined with the biochemical parameters associated with mitochondrial function, histological observation under an electron microscope, western blotting, immunofluorescence and other indicators. A comprehensive study of the neuroprotective effects of DBD revealed potential biomarkers related to the disorder of the mitochondrial metabolic pathways. Finally, the present study performed targeted metabolic profiling and validated potential therapeutic targets.

## Materials and methods

**Animals.** A total of 63 male-specific pathogen-free SD rats (5-8 weeks-old; 250-280 g weight) were purchased from

the Hunan Shrek Jingda Experimental Animal Co., Ltd. [Laboratory animal qualification certificate: scxk (Xiang) 2019-0004]. The rats had free access to food and water; the feeding environment was maintained in a 12-h light/dark cycle, at a temperature of 20-23°C and a relative humidity of 40-60%. All animal experiments were approved by the Animal Ethics Committee of Yunnan University of Traditional Chinese Medicine (approval no. R-062021088) and the care and use of experimental animals were in accordance with the guidelines of the National Institutes of Health. Prior the experiment, the rats were randomly categorized into sham (Sham), model (MCAO/R) and treat (MCAO/R + DBD 10 mg/kg) groups, with 21 rats in each group. DBD ( $\geq 98\%$  purity) was purchased from Chengdu Alfa Biotechnology Co., Ltd. Based on the effective doses determined in our previous study (17), the treat group was continuously given 10 mg/kg by gavage for 7 days, whereas the model and sham groups were given the same amount of distilled water by gavage.

**MCAO/R model.** The MCAO/R model was replicated by the suture method as described previously (26) with slight modifications. In brief, rats were anesthetized by intraperitoneal injection of 2% sodium pentobarbital (40 mg/kg). The right common carotid artery (CCA) and vagus nerve of the rats were isolated and a 0.36-mm-diameter polynylon monofilament with a rounded tip (cat. no. 2636-50A4; Beijing Cinontech Co., Ltd.) was inserted into the middle cerebral artery from the CCA through the internal carotid artery; the insertion was stopped if a slight resistance was encountered ( $\sim 18$ -20 mm). After 2 h of ischemia, the middle cerebral artery was reperfused by gently pulling the suture back to the CCA. The sham group underwent the same process except for suture blockage. Neurological scoring was performed at 24 h after reperfusion. During this period, none of the animals developed humane endpoint indications, such as non-feeding, dyspnea and hypothermia, or died prematurely. Neurological deficit was assessed on a scale of 0-4 points: 0 points: regular activity, no neurological deficit; 1 point, when the tail is lifted, the left forelimb is adducted and cannot be fully extended; 2 points, the body rotates to the left when crawling; 3 points, the body tilts to the left when crawling; 4 points, inability to walk spontaneously with a decreased level of consciousness (26). The inclusion criterion for this model was a neurological score of 1-3; those with scores of 0 or 4 were excluded.

**Measurement of cerebral infarct area.** After 24 h of I/R, the rats were injected intraperitoneally with 2% sodium pentobarbital (150 mg/kg) to induce deep anesthesia and no response to tail entrapment. Then the animals were rapidly sacrificed using a decapitation device. The whole brains were removed and frozen at -20°C for 20 min. Coronal sections from front to back (2 mm) were made on the brains on ice, stained with 2% triphenyl tetrazolium chloride (TTC) (cat. no. A610558; Sangon Biotech Co., Ltd.) in the dark for 20 min at 37°C and then fixed in 4% paraformaldehyde for 24 h at room temperature. The infarcted areas were analyzed with ImageJ 1.52 a (National Institutes of Health).

**Hematoxylin and eosin (HE) staining.** The prepared brain tissue paraffin sections were heated at 60°C for 3 h. Hematoxylin

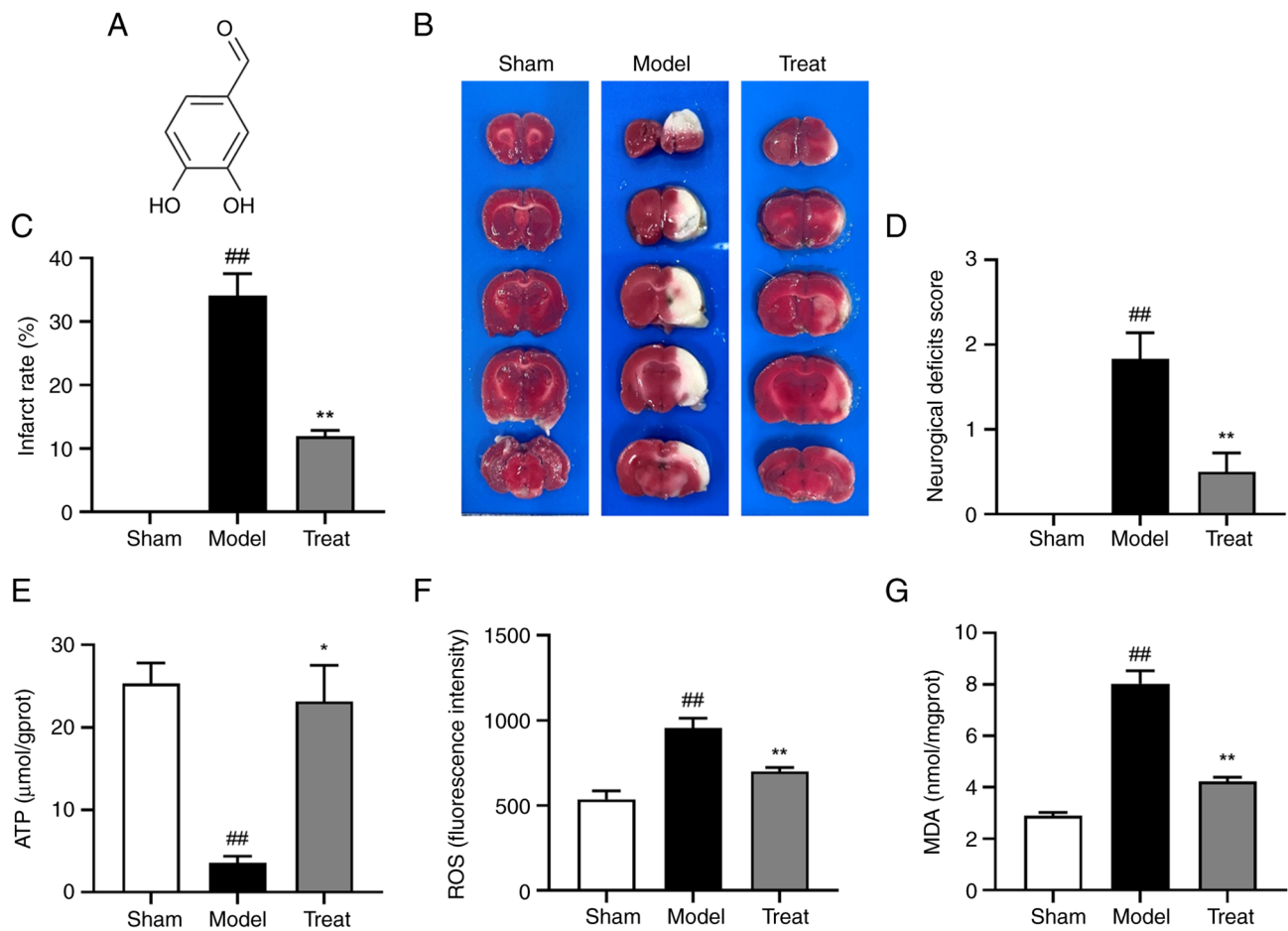


Figure 1. DBD has a protective effect on cerebral I/R injury. (A) Chemical structure of DBD. (B) Representative images of brain sections stained with TTC to visualize infarcts. Red is normal tissue and white is infarcted. (C) Quantitative analysis of infarct size. (D) Neurological deficit scores in different groups. (E) ATP content of brain tissue. Oxidative stress-related indicators (F) ROS level and (G) MDA content. All data are presented as the mean  $\pm$  standard error of the mean, n=6. <sup>##</sup>P<0.01 vs. Sham group; <sup>\*</sup>P<0.05, <sup>\*\*</sup>P<0.01 vs. Model group. DBD, 3,4-Dihydroxybenzaldehyde; I/R, ischemia/reperfusion; TTC, triphenyl tetrazolium chloride; ATP, adenosine triphosphate; ROS, reactive oxygen species; MDA, malondialdehyde.

was administered for 2 min and then washed off; the sections were stained with eosin dye for 1 min at room temperature. The samples were dehydrated and dried with graduated alcohol series, cleared with xylene to make and sealed with neutral gum. Images were captured using an inverted phase contrast microscope (IXplore; OM Digital Solutions Corp.) under a field of view of x400 magnification. A HE staining kit was used for histomorphological analysis (cat. no. KGA224; Nanjing KeyGen Biotech Co., Ltd.).

**Immunofluorescence staining.** Brain sections were dewaxed, dried at 60°C for 60 min, dewaxed twice with xylene and hydrated with ethanol (100, 95, 80 and 75%) for 5 min each time. Proteinase K working solution (100 μl) was added dropwise to each tissue section and incubated at 37°C for 30 min. Next, 50 μl of TUNEL fluorescence detection solution was added to each sample. Then, the sample was incubated at 37°C for 60 min in the dark. Nuclei were counterstained with DAPI for 5 min at room temperature. Observed the cortex from the cerebral under a laser confocal microscope (Zeiss LSM; Carl Zeiss AG) and images captured at 400x magnification (n=3). The areas of interest were then cropped to approximately 50 μm for presentation. All analyses were performed in a blinded manner. The

TUNEL detection kit (cat. no. C1090; Beyotime Institute of Biotechnology).

**Transmission electron microscopy.** After 24 h of I/R, the rats were euthanized and ~1-mm<sup>3</sup> of the brain tissue isolated from the ischemic cortex from the cerebral infarction area was collected, fixed with 4% glutaraldehyde and then post-fixed with 1% osmic acid at 4°C for 2 h. The samples were dehydrated using graduated alcohol series and acetone, embedded in epoxy resin at 60°C incubator for 48 h, sliced into 80 nm-thick sections and stained with 4% ethyl citrate uranyl for 15 min at room temperature. The ultrastructure of mitochondria was observed and randomly selected fields of view were captured at 400x magnification (n=3) using transmission electron microscopy (JEM-1400flash; JEOL Ltd.).

**Extraction and index determination of rat brain mitochondria.** Based on the regions identified in a previous study (27), 200 mg of the cortical tissue of the ischemic hemisphere was collected following MCAO/R for 24 h. The blood was rinsed with normal saline, dried using a filter paper, cut into pieces and placed in a 2 ml glass homogenizer for homogenization. High-purity mitochondria were extracted using a commercially available mitochondrial extraction kit (cat. no. SM0020;

Beijing Solarbio Science & Technology Co., Ltd.) according to the manufacturer's instructions and stored at  $-80^{\circ}\text{C}$ . The specific operation steps were as follows: Centrifugation at  $4^{\circ}\text{C}$ ,  $1,000 \times g$  for 5 min, transferring the supernatant to a new centrifuge tube at  $4^{\circ}\text{C}$ ,  $1,000 \times g$  for 5 min, continuing to remove the supernatant and transferring to the new centrifuge tube,  $4^{\circ}\text{C}$ ,  $12,000 \times g$  for 10 min. The supernatant, after centrifugation, contained cytoplasmic components, while the mitochondria precipitated at the bottom of the tube. After removing the supernatant, 0.5 ml Wash Buffer was added to the mitochondrial precipitation and centrifuged at  $4^{\circ}\text{C}$   $1,000 \times g$  for 5 min. Then the supernatant was transferred to a new centrifuge tube for 10 min at  $4^{\circ}\text{C}$  and  $12,000 \times g$ . Finally, the supernatant was removed and the high-purity mitochondria were precipitated at the bottom of the tube. Subsequently, the mitochondrial purity was evaluated. Purified mitochondria and non-purified mitochondrial suspension (mitochondria not treated with wash buffer in mitochondrial extraction kit and containing other cell tissues) were mixed with  $100 \mu\text{l}$  each of 0.3% Janus green B (mitochondria specific staining; cat. no. S19083, Shanghai Yuanye Bio-Technology Co., Ltd.) and 0.15% neutral red solution (lysosomal and Golgi staining; cat. no. DN300; Beijing Dingguo Changsheng Biotechnology Co., Ltd.). The purified and non-purified mitochondria samples from the cerebral cortex ( $n=3$ ) were stained for 10 min at room temperature and then observed and randomly selected fields of view under an optical microscope at  $400\times$  magnification (DMi1; Leica Microsystems, Inc.).

A mitochondrial protein Extraction kit (cat. no. G008-1; Nanjing Jiancheng Bioengineering Institute) was used to extract total protein from the isolated mitochondria. Then, the protein content of each sample was determined using a BCA protein quantification kit (cat. no. PC0020; Beijing Solarbio Science & Technology Co., Ltd.). Additionally, ATP content in brain tissue was determined using an ATP assay kit (cat. no. A095-1-1; Nanjing Jiancheng Bioengineering Institute). The oxidation indexes of brain tissue and the level of reactive oxygen species (ROS) were detected by using DCFH-DA as the fluorescent probe (cat. no. E004-1-1; Nanjing Jiancheng Bioengineering Institute). Malondialdehyde (MDA) content was detected using the thiobarbituric acid method (cat. no. BC0025; Beijing Solarbio Science & Technology Co., Ltd.). For the detection of brain mitochondrial function indicators, the mitochondrial respiratory chain complex I-IV activity detection kit (cat. nos. BC0515, BC3235, BC3245 and BC0945; Beijing Solarbio Science & Technology Co., Ltd.) was used. The electron transport chain (ETC) contains four multisubunit enzyme complexes, including mitochondria complex I (nicotinamide adenine dinucleotide dehydrogenase, NADH dehydrogenase), mitochondria complex II (succinate dehydrogenase), mitochondria complex III (cytochrome c reductase) and mitochondria complex IV (cytochrome c oxidase). The mitochondrial swelling method was used to measure the opening degree of mPTP. The MMP level was measured by fluorescence spectrophotometry (cat. nos. GMS10101 and GMS10013.1, Shanghai Genmed Gene Medicine Technology Co., Ltd.). The content of cytochrome c (Cyt-c) in brain mitochondria was measured using ELISA kit (H190-1-1, NanJing JianCheng Bioengineering Inc.).

*Western blotting.* RIPA lysis buffer (PSMF:RIPA lysis buffer=1:100; cat. nos. 042121210730; 051021210825; Beyotime Institute of Biotechnology) was added to the treated brain tissue and lysed on ice for 20 min and the lysed product was centrifuged at  $14,200 \times g$  for 5 min at  $4^{\circ}\text{C}$ . Protein quantification was performed by the BCA method. Equal amounts of protein ( $80 \mu\text{g}$ ) were separated by 8% SDS-PAGE and transferred to PVDF membranes. Electrophoresis was performed at 80 V for  $\sim 30$  min. After the protein marker was separated and the sample entered the separation gel, the parameter was changed to a constant voltage of 120 V. After electrophoresis, the membrane was transferred until the target band reached the appropriate position. The membrane was blocked with 5% bovine serum albumin (SW3015, Beijing Solarbio Science & Technology Co., Ltd.) at room temperature for 1 h. After blocking, the membrane was washed twice with TBST buffer (0.1% Tween; cat. no. QN1236; Beijing Biolab Technology Co., Ltd.). Subsequently, the membrane was incubated with primary antibodies, including Bax (1:1,000; cat. no. 50599-2-Ig; ProteinTech Group), Bcl-2 (1:500; cat. no. 26593-1-AP; ProteinTech Group), Caspase-3 (1:1,000; cat. no. 9662; Cell Signaling Technology, Inc.), O-GlcNAc transferase (OGT; 1:500; cat. no. 61355, Active Motif, Inc.) and  $\beta$ -Actin (1:25,000; cat. no. 66009-1-Ig; ProteinTech Group, Inc.), overnight at  $4^{\circ}\text{C}$ . Then, it was incubated with goat anti-rabbit IgG and Rabbit Anti-Mouse IgG secondary antibodies (both at 1:5,000, cat. nos. ab6721 and ab97046, Abcam) for 1 h at room temperature. The immunoreactive bands were developed using enhanced chemiluminescence reagent (cat. no. A38555; Thermo Fisher Scientific, Inc.) and images were captured in the Bio-Rad ChemiDoc XRS gel imaging system (Bio-Rad Laboratories, Inc.). ImageJ Lab V4.0 software (Bio-Rad Laboratories, Inc.) was used for quantitative analysis.

*Brain sample preparation and extraction.* After 2 h of ischemia and 24 h of reperfusion, the rats were sacrificed and 200 mg of the cortical tissue samples of the infarcted hemisphere was quickly collected and stored at  $-80^{\circ}\text{C}$  for later use. A total of six brain tissue samples were collected from each group. After the sample was thawed and homogenized, 0.05 g of the sample was mixed with  $500 \mu\text{l}$  of 70% methanol/water. The sample was vortexed for 3 min at  $2,500 \text{ rpm}$  and centrifuged at  $14,200 \times g$  for 10 min at  $4^{\circ}\text{C}$ . Afterwards,  $300 \mu\text{l}$  of supernatant was collected into a new centrifuge tube and placed in a  $-20^{\circ}\text{C}$  refrigerator for 30 min. Then, the supernatant was centrifuged again at  $14,200 \times g$  for 10 min at  $4^{\circ}\text{C}$ . After centrifugation,  $200 \mu\text{l}$  of supernatant was transferred through protein precipitation plate for further LC-MS analysis. Each group of  $20 \mu\text{l}$  samples was mixed as quality control (QC) samples. Analyzing the coefficient of variation (CV) of QC samples, the CV value indicates the ratio of the standard deviation of the original data to the mean of the actual average data, reflecting the degree of data dispersion. Furthermore, indicating the stability of experimental data was tested to ensure QC.

#### *UPLC-MS/MS system conditions*

*UPLC conditions.* Amide method: HPLC was performed under the following conditions: Column, ACQUITY UPLC BEH Amide (Waters Corporation; i.d.  $2.1 \times 100 \text{ mm}$ ,  $1.7 \mu\text{m}$ ); solvent system, water with 10 mM of ammonium acetate and 0.3%

ammonium hydroxide (A) and 90% acetonitrile/water (v/v) (B). The gradient was started at 95% B (0-1.2 min), decreased initially to 70% B (8 min) and then to 50% B (9-11 min) and finally ramped back to 95% B (11.1-15 min) under the following conditions: Flow rate, 0.4 ml/min; temperature, 40°C; injection volume, 2  $\mu$ l.

**ESI-MS/MS conditions.** Linear ion trap and triple quadrupole scans were acquired using a triple quadrupole-linear ion trap mass spectrometer (QTRAP), QTRAP 6500+ LC-MS/MS System (Sciex), operating in positive and negative ion mode. The ESI source operation parameters were as follows: ion source, ESI+/-; source temperature, 550°C; ion spray voltage 5,500 V (positive) and -4,500 V (negative); curtain gas was set at 35 psi. Tryptophan and its metabolites were analyzed using scheduled multiple reaction monitoring. Data acquisitions were performed using Analyst 1.6.3 (Sciex). Multiquant 3.0.3 (Sciex) was used to quantify all metabolites.

**Data processing and statistical analysis.** Unsupervised principal component analysis (PCA) was performed by statistics function prcomp V1.0.1 (r-project.org) within R (www.r-project.org). Data were unit variance scaled before unsupervised PCA. The hierarchical cluster analysis results of samples and metabolites were presented as heatmaps with dendrograms using R package pheatmap V1.2.1 (r-project.org). Significantly regulated metabolites among groups were determined by variable importance in projection (VIP) and absolute  $\text{Log}_2\text{FC}$  (fold change). VIP-values were extracted from orthogonal partial least squares discriminant analysis (OPLS-DA) result and generated using R package MetaboAnalystR V1.0.1 (28). P-value of the unpaired student's test determined their significance. Metabolites were annotated using the KEGG database and then mapped to the KEGG pathway database (<http://www.kegg.jp/kegg/pathway.html>). Then, the pathways to which the metabolites with significant modulation were mapped were fed into metabolite set enrichment analysis and the P-value of the hypergeometric test determined their significance.

GraphPad Prism 9.0.0 (GraphPad Software, Inc.) was used for statistical analyses. The data conform to the normal distribution. If the variance was homogeneous, then it was analyzed with Bonferroni's multiple comparisons test using one-way analysis of variance (ANOVA). If the variance is unequal, then it was analyzed Dunnett's T3 multiple comparisons test in Welch's ANOVA test. Non-normally distributed data were analyzed with Dunn's multiple comparisons test in the Kruskal-Wallis test. All values were presented as mean  $\pm$  standard error of the mean.  $P < 0.05$  was considered to indicate a statistically significant difference.

## Results

**DBD effectively improves MCAO/R in rats.** TTC staining reflects cerebral infarction after injury and the area of ischemic necrosis is stained white (29). The results showed that obvious white infarcts in the model group after cerebral I/R and DBD could significantly reduce the infarct volume (Fig. 1B and C). Compared with the model group, the neurological function of the rats in the DBD group was significantly improved (Fig. 1D). Among them, the ATP content in the brain tissue

of MCAO/R rats was significantly decreased, but this was reversed by DBD (Fig. 1E). In addition, the levels of oxidative stress-related indicators ROS and MDA increased following I/R, while DBD could significantly inhibit the generation of ROS and MDA (Fig. 1F and G). DBD effectively attenuated brain injury and oxidative stress in MCAO/R rats while restoring energy supply.

**DBD can alleviate mitochondrial damage induced by MCAO/R.** At the heart of mitochondrial dysfunction is ATP reduction and to determine the effect of DBD on mitochondrial damage, follow-up experiments were performed. Observation of mitochondrial ultrastructure in neurons from the cortex tissue was performed using transmission electron microscopy. It was shown that I/R resulted in severe swelling of mitochondria and partial disappearance of cristae, rupture of inner and outer membranes (the matrix is electron transparent). By contrast, DBD ameliorated this injury, leaving the inner and outer membranes and ridges largely intact with only mild swelling (Fig. 2A). Then, high-purity mitochondria were isolated by gradient centrifugation for detection of related indexes. Microscopic examination revealed a number of dark reds in non-purified mitochondria and a single blue-green color in purified mitochondria (Fig. S1). These results indicated that the purity of the extracted mitochondria was high. Following brain I/R, the activity of mitochondrial respiratory chain enzyme complexes I-IV was inhibited. Mitochondrial respiratory chain enzyme complexes I and II can oxidize NADH produced by the TCA cycle and the oxidation of succinate, respectively and donate electrons to ETC (30). Complex III reduces the mobile electron carrier Cyt-C, ferries single electrons that are subsequently transferred from complex III to complex IV, where molecular oxygen is bound and reduced to water (31). This electron transfer chain provides an electrochemical gradient across the inner mitochondrial membrane to drive ATP synthesis. In addition, ROS are mainly formed by premature leakage of electrons from complexes I, II and III (31). mPTP was abnormally opened and MMP level and mitochondrial Cyt-c content were decreased. However, DBD had a positive effect on mitochondrial health in MCAO/R rats, manifested by increased activity of mitochondrial respiratory chain enzyme complexes I-IV (Fig. 2B-E), restored mPTP levels (Fig. 2F), addition to decreased MMP loss (Fig. 2G) and increased mitochondrial Cyt-c content (Fig. 2H). Experiments showed that DBD alleviated cerebral I/R injury, which may restore cellular energy supply by improving mitochondrial dysfunction, thereby inhibiting the transfer of mitochondrial Cyt-c to the cytoplasm, reducing apoptosis and protecting neurons.

**Metabolomic analysis of MCAO/R rats following DBD treatment.** Evaluation of QC samples showed that the proportion of substances with CV values less than 0.5 in the test and QC samples were higher than 85%, indicating that the experimental data was stable (Fig. 3). To understand the changes on metabolites in I/R of DBD treatment more clearly, the sham group cortical tissue of rats and model and treat cerebral cortical tissue of the ischemic hemisphere ( $n=6$ ) were collected for metabolic study. Analyst 1.6.3 software (Sciex) was used to process LC-MS data and to obtain the total ion

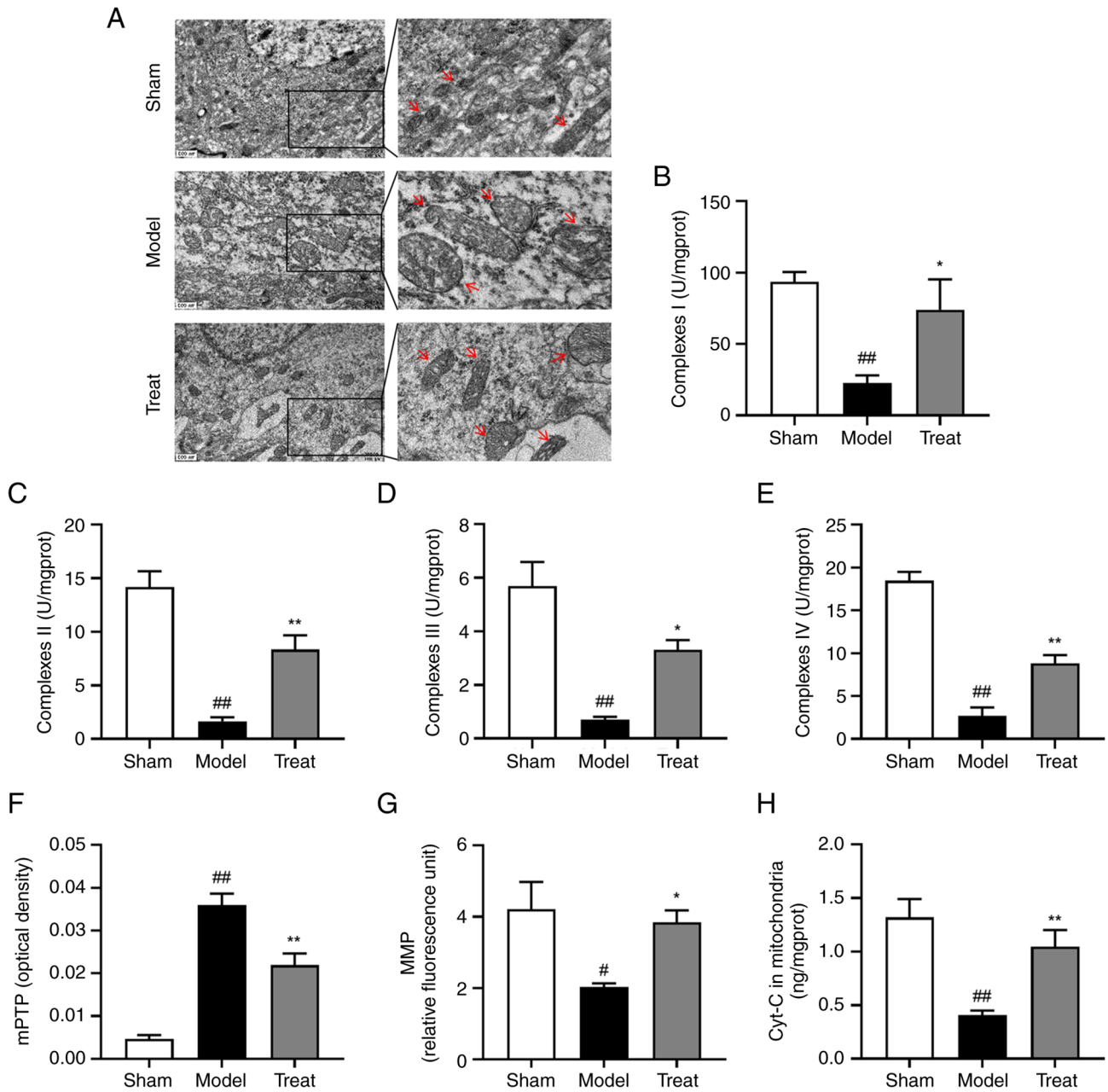


Figure 2. DBD has a protective effect on mitochondrial brain damage. (A) Electron microscope observation of the structure and morphology of mitochondria in different groups of brain tissues; the right image is the enlarged image in the left panels. Red arrows indicated typical changes in mitochondrial morphology. Magnification, x400; scale bar=500 nm. The activity of mitochondrial respiratory chain enzyme complexes (B) I, (C) II, (D) III, and (E) IV in each group. (F) The mitochondrial swelling method determined the degree of mPTP opening and the higher the mitochondrial swelling value, the greater the opening degree of mPTP. (G) MMP levels, a decrease in MMP is an early signal of apoptosis. (H) mitochondrial Cyt-c content, an essential protein in apoptosis and an important mediator in the mitochondrial respiratory chain can reflect apoptosis. All data are presented as the mean ± standard error of the mean, n=6. Scale bar=500 nm #P<0.05, ##P<0.01 vs. Sham group; \*P<0.05, \*\*P<0.01 vs. Model group. DBD, 3,4-Dihydroxybenzaldehyde; mPTP, mitochondrial permeability transition pore; Cyt-c, cytochrome c.

chromatogram of all samples (Figs. S2-S4). In addition, a total of 57 metabolites were detected based on the UPLC-MS/MS detection platform and database, including 17 nucleotides and their metabolites, 12 amino acids, 10 Organic acids and their derivatives, eight phosphate sugars, five phosphoric acids, three coenzymes and vitamins, one lysophosphatidylethanolamine and amino acid derivatives.

Principal component analysis and heatmap clustering was used to examine all metabolites in the data. The PCA results showed clear separation among the different treatments

(Fig. 4A), indicating that the metabolites of samples changed significantly following MCAO/R, consistent with the I/R phenotype. The change was mainly dominated by the first principal component (PC1) of the X-axis, which can explain 45.82% of the characteristics of the original data set. From PC1, it can be found that the model group and the treatment group are separated and that there are differences between them.

The differences in the accumulation patterns of metabolites in the sham-operated group, the model group and the treatment

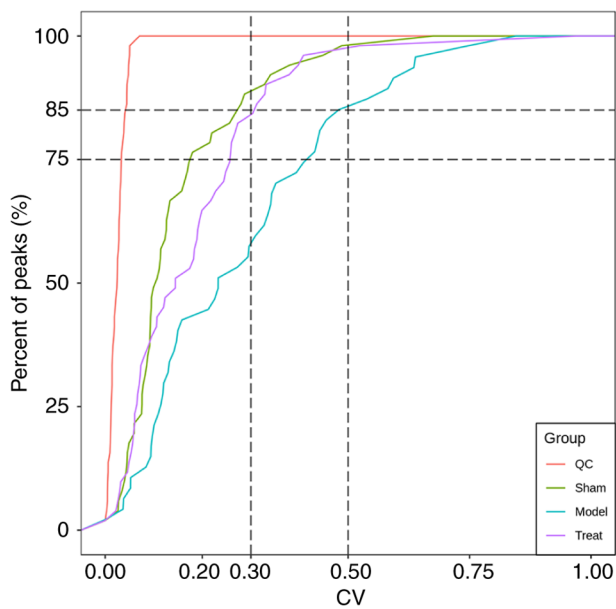


Figure 3. CV distribution map in each group of samples. Red lines represent QC samples, green represent Sham samples, blue represents Model samples and purple represents Treat samples. The reference lines perpendicular to the X-axis correspond to CV values of 0.3 and 0.5. The two parallel to the X-axis corresponds to 75 and 85% of the total number of substances. CV, the coefficient of variation.

group can be analyzed by clustering heatmaps (Fig. 4B). The results showed significant differences in substances in different groups, which were divided into two clusters. The metabolites in cluster 1 were the highest in the sham operation group, medium in the treatment group and the model group. The lowest content, including most nucleotides and their metabolites, such as adenosine monophosphate (AMP), ATP, adenosine diphosphate (ADP), guanosine and uracil, decreased following MCAO/R, which may result from inhibited energy production. The metabolites in cluster 2 were highest in the model group, moderate in the treatment group and lowest in the sham group. Among them, the increased expression of phosphoenolpyruvic acid in the gluconeogenesis pathway after IS was mainly found in astrocytes, which can promote acidosis and oxidative damage, resulting in disturbance of glucose metabolism during I/R (32). The same excess of 3-phenyllactic acid (PLA) has also been shown to induce ROS production in glial cell (33). In addition, ornithine, L-citrulline, L-leucine and other essential amino acids increased in MCAO/R, which may be the accumulation of protein synthesis disorders. The different biological replicates also clustered together, indicating good homogeneity between biological replicates and high data reliability.

**Analysis of differential metabolites between model group and treatment group.** OPLS-DA analysis is a multivariate statistical analysis method with supervised pattern recognition, which can effectively eliminate influences irrelevant to the present study to screen differential metabolites. OPLS-DA was used to perform a pairwise analysis of the three groups to draw a score map. In this model,  $R^2X$  and  $R^2Y$  represented the interpretation rate of the X and Y matrices of the built model, respectively, and  $Q^2$  represented the predictive ability of the

model.  $Q^2$  were all higher than 0.9,  $P < 0.05$ , indicating that the constructed model was suitable (Fig. 5A). The OPLS-DA score plot showed that there was a clear separation between the model group and the treatment group (Fig. 5B). Fold Change (FC) and VIP was used to screen differential metabolites, metabolites satisfying  $FC \geq 2$  and  $FC \leq 0.5$  and  $VIP \geq 1$  were considered to have significant differences and the screening results were displayed in a volcano plot (Fig. 5C). The results showed that in the comparison between the model group and the treatment group, there were a total of nine differential metabolites, of which eight metabolites were upregulated: Succinyl-CoA, UDP-GlcNAc, deoxythymidine monophosphate (dTMP), AMP, inosine monophosphate (IMP), uridine 5'-monophosphate (UMP), fructose 1,6-bisphosphate, 6-phosphogluconic acid; 1 metabolite was downregulated: 3-phenyllactic acid (Fig. 5D; Table I).

To comprehensively observe changes in metabolic pathways, the present study employed a pathway-based metabolic change analysis method, Differential Abundance (DA) Score, which captures the overall changes of all metabolites in a pathway (Fig. 5E). The differential metabolites between the model group and the control group were mainly annotated and enriched in fructose and mannose metabolism, tropane, piperidine and pyridine alkaloid biosynthesis, amino sugar and nucleotide sugar metabolism and pentose phosphate pathway. These pathways interact and are closely related to I/R. Based on the results described above, a metabolite overview of key pathways in brain tissue is shown in (Fig. 6).

**Presentation of quantitative results of UDP-GlcNAc and verification of OGT expression following DBD treatment.** The most significantly differential metabolite induced by DBD was UDP-GlcNAc and OGT is the key catalytic enzyme of UDP-GlcNAc. Subsequently, the content of UDP-GlcNAc in the brain detected by metabolomics was visualized and the protein expression of OGTase detected. The experimental results showed that compared with the sham-operated group, the range of UDP-GlcNAc in the model group was reduced, which could be improved by DBD (Fig. 7A). Western blotting results showed that the expression of OGT was significantly increased following DBD treatment compared with the model group (Fig. 7B). This indicated that DBD increased the level of UDP-GlcNAc in the brain after IS by promoting the expression of OGT.

**DBD inhibits MCAO/R-induced apoptosis of brain cells.** Apoptosis is the final and primary determinant of brain I/R injury. In HE staining, the brain tissue cells of the rats in the Sham group were arranged neatly and their morphological structures were normal. In the model group, the gap of cell structure was widened, nuclear pyknosis appeared, and the fiber arrangement was disordered, while the treat group exhibited improved pathology of brain tissue (Fig. 8A). TUNEL staining showed that MCAO/R decreased the number of neurons and increased the number of positive apoptotic cells. Following DBD treatment, apoptotic cells were significantly reduced (Fig. 8B and C). In addition, the protein expression of genes related to apoptosis was analyzed by western blotting (Fig. 8D-H). MCAO/R induced the up-regulation of Bax and cleaved-Caspase-3 and the downregulation of Bcl-2.

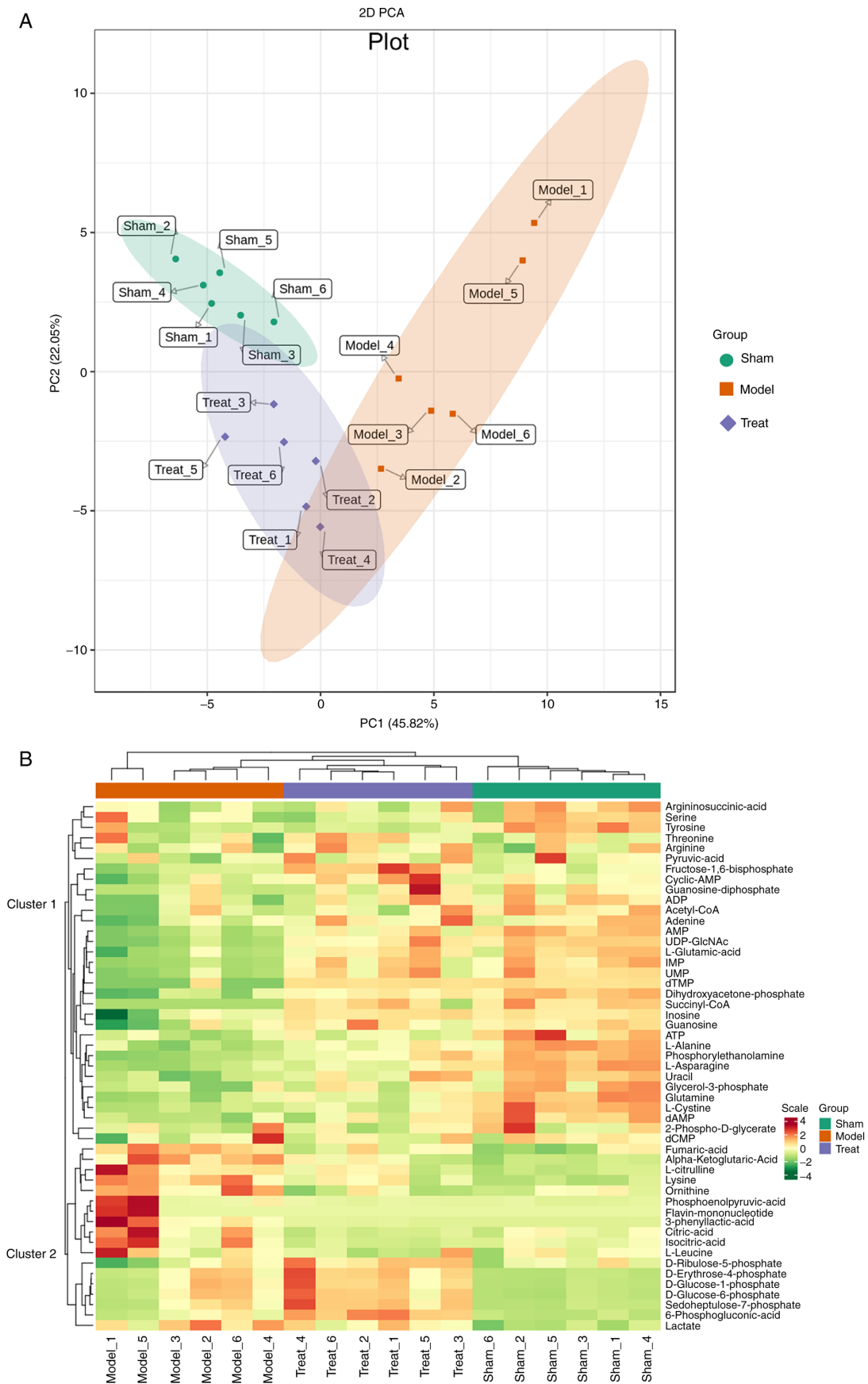


Figure 4. PCA of metabolomic changes in each group and cluster heat map of metabolites were performed based on LC-MS/MS system. (A) In the PCA diagram of each group, each point represents a sample and color represents the samples in the same group. Green: Sham group, Red: Model group, Purple: Treat group. The Sham and Model groups were clearly divided, indicating that the metabolites in the samples following MCAO/R changed significantly. (B) Sample overall clustering heat map, where the clustering line on the left is the metabolite clustering line and the upper one is the sample clustering line. Scale is the expression level after normalization (the redder the color, the higher the expression level). PCA, principal component analysis; MCAO/R, middle cerebral artery occlusion/reperfusion.

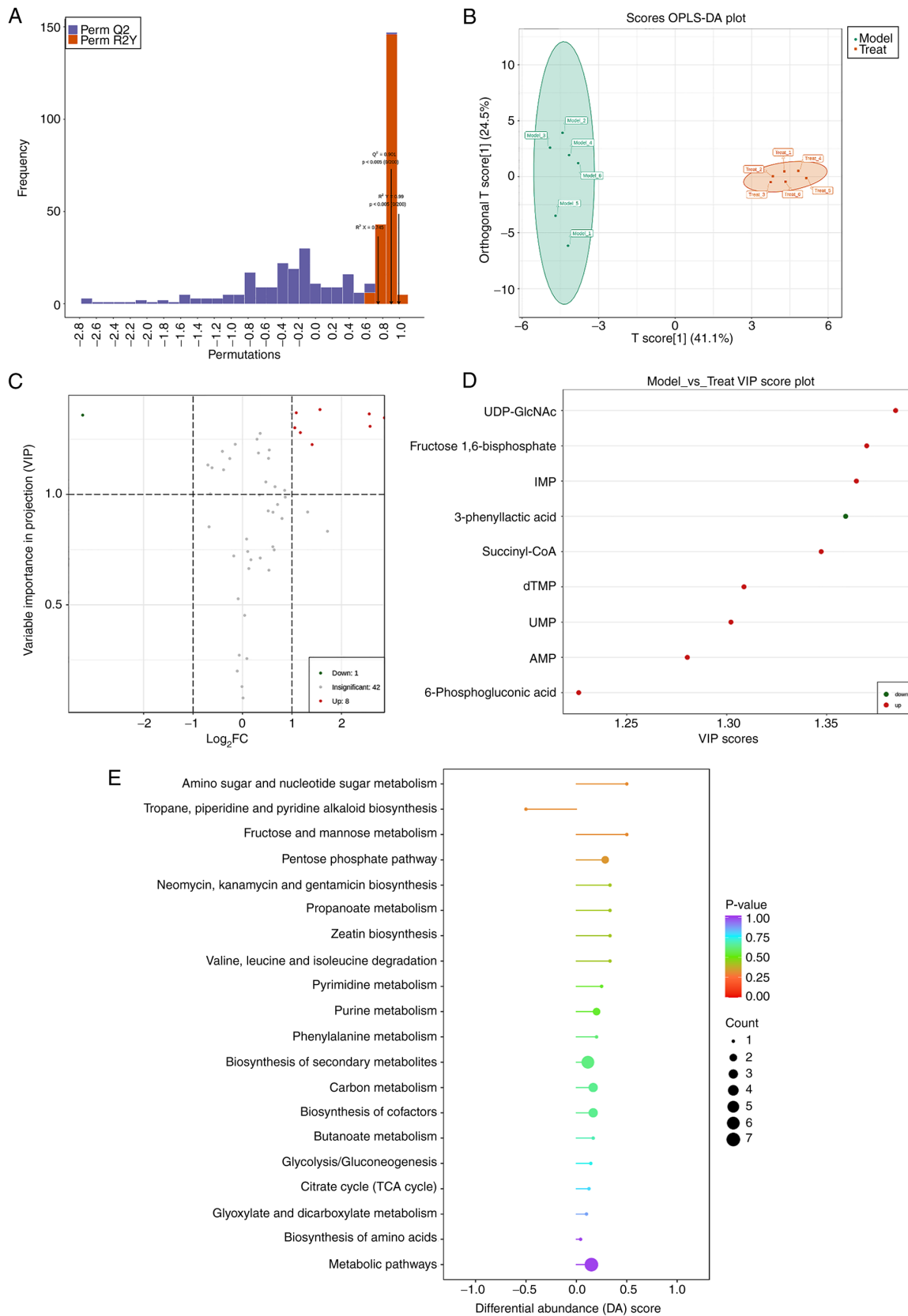


Figure 5. The enrichment analysis of differential metabolites and metabolic pathways following MCAO/R analysis by OPLS-DA. (A) OPLS-DA model validation plot, usually Q2, is higher than 0.9 and the model is best when  $P < 0.05$ . (B) OPLS-DA score plot, representing the gap between Model group and Treat group. Green: Model group, Red: Treat group. (C) Volcano plot of differential metabolites, the greater the absolute value of the abscissa, the greater the fold difference in expression between the Model group and the Treat group. The greater the ordinate value, the more significant the differential expression. Green dots: Downregulated metabolites, red: upregulated metabolites and visualized in (D) Differential metabolite score plot ( $VIP \geq 1$ ). (E) DA score plot of differential metabolic pathways. The dots are distributed on the left side of the central axis. The longer the line segment, the more the pathway's overall expression tends to be up-regulated; the larger the dots, the more metabolites and vice versa. The color reflects the size of the P-value; red, the smaller the P-value. MCAO/R, middle cerebral artery occlusion/reperfusion; OPLS-DA, orthogonal partial least squares discriminant analysis; VIP, variable importance in projection; DA, discriminant analysis.

Table I. Screening results of differential metabolites in Model group and Treat group.

Metabolites	Formula	RT (min)	VIP	Fold change	P-value	Type
UDP-GlcNAc	C <sub>17</sub> H <sub>27</sub> N <sub>3</sub> O <sub>17</sub> P <sub>2</sub>	4.47	1.385	2.960	4.16x10 <sup>-4</sup>	Up
Fructose 1,6-bisphosphate	C <sub>6</sub> H <sub>14</sub> O <sub>12</sub> P <sub>2</sub>	6.98	1.370	2.123	4.21x10 <sup>-4</sup>	Up
IMP	C <sub>10</sub> H <sub>13</sub> N <sub>4</sub> O <sub>8</sub> P	5.34	1.365	5.905	2.78x10 <sup>-3</sup>	Up
3-phenyllactic acid	C <sub>9</sub> H <sub>10</sub> O <sub>3</sub>	0.52	1.360	0.106	4.89x10 <sup>-2</sup>	Down
Succinyl-CoA	C <sub>25</sub> H <sub>40</sub> N <sub>7</sub> O <sub>19</sub> P <sub>3</sub> S	5.61	1.347	Inf	5.45x10 <sup>-3</sup>	Up
dTMP	C <sub>10</sub> H <sub>15</sub> N <sub>2</sub> O <sub>8</sub> P	4.62	1.309	5.973	4.16x10 <sup>-3</sup>	Up
UMP	C <sub>9</sub> H <sub>13</sub> N <sub>2</sub> O <sub>9</sub> P	5.21	1.302	2.080	3.35x10 <sup>-3</sup>	Up
AMP	C <sub>10</sub> H <sub>14</sub> N <sub>5</sub> O <sub>7</sub> P	5.25	1.280	2.248	2.06x10 <sup>-3</sup>	Up
6-Phosphogluconic acid	C <sub>6</sub> H <sub>13</sub> O <sub>10</sub> P	6.13	1.226	2.650	3.65x10 <sup>-4</sup>	Up

UDP-GlcNAc, uridine diphosphate N-acetylglucosamine; IMP, inosine monophosphate; dTMP, deoxythymidine monophosphate; UMP, uridine monophosphate; AMP, adenosine-monophosphate.

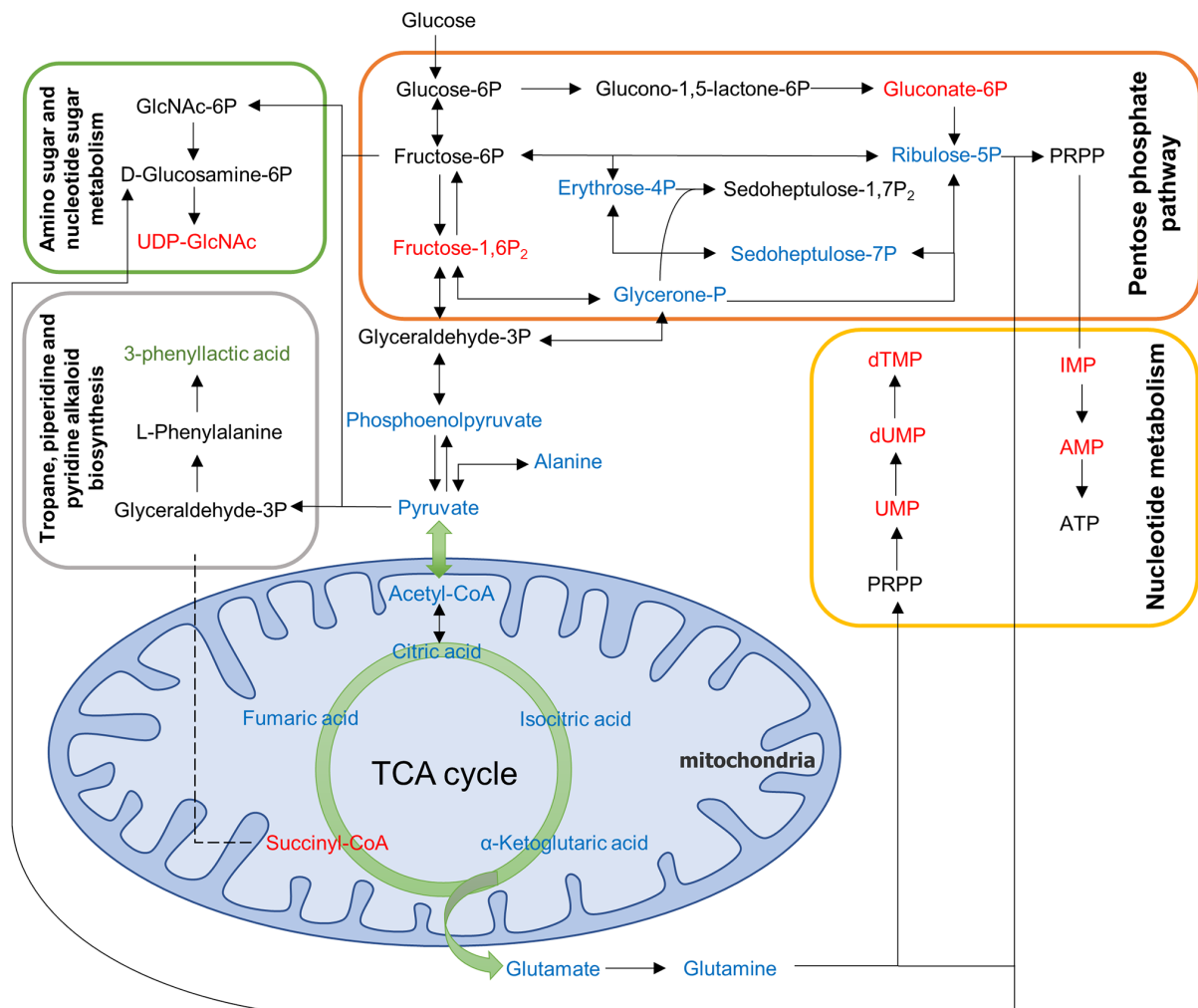


Figure 6. Graph of the central metabolic network with significant changes following MCAO/R. Compared with the Model group, elevated metabolites in the Treat group are indicated in red, decreased metabolites in green, and detected but not significant metabolites in blue. MCAO/R, middle cerebral artery occlusion/reperfusion; TCA, tricarboxylic acid cycle.

However, DBD partially reversed MCAO/R-induced apoptosis compared with the MCAO/R group. It was hypothesized that DBD inhibits MCAO/R-induced brain cell apoptosis and reduces neuronal loss caused by cerebral I/R injury.

## Discussion

The present study attempted to identify the neuroprotective effect of DBD on cerebral I/R injury and the underlying

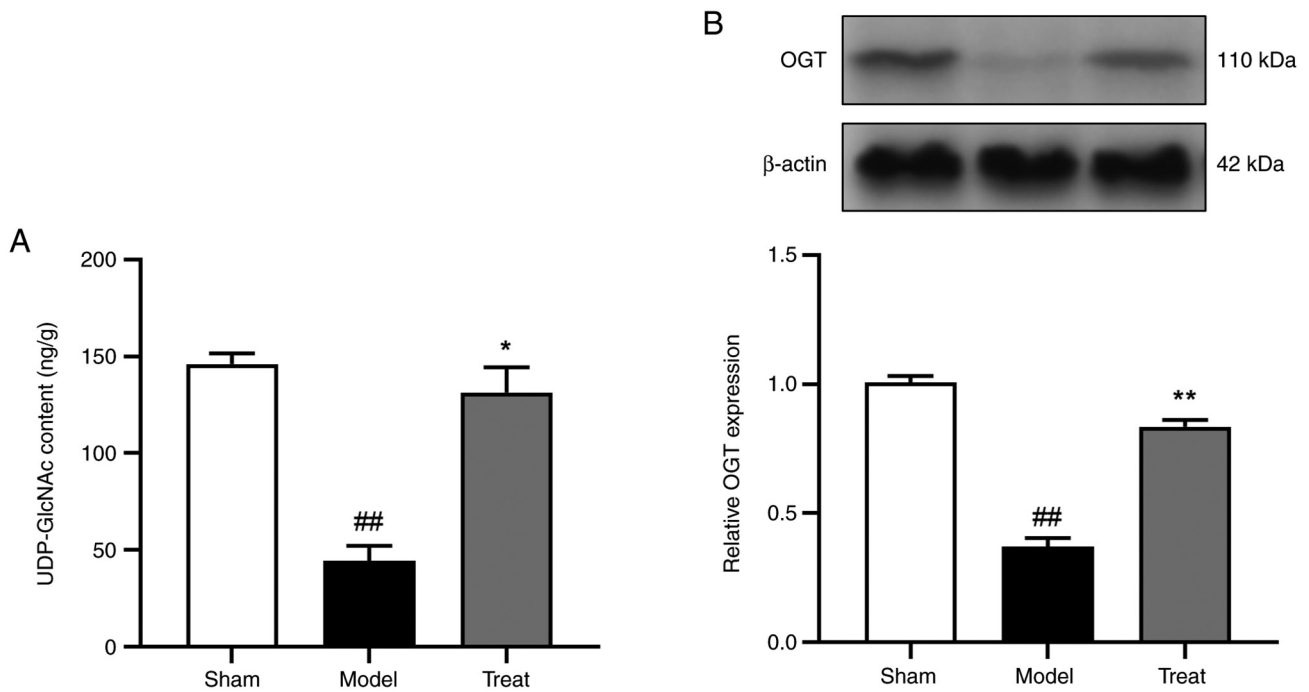


Figure 7. Effects of DBD on UDP-GlcNAc and OGT in MCAO/R rats. (A) Quantitative results of the metabolite UDP-GlcNAc in each group. (B) Representative western blotting and quantitative analysis of OGT expression. All data are presented as the mean  $\pm$  standard error of the mean,  $n=3$ . ## $P<0.01$  vs. Sham group; \* $P<0.05$ , \*\* $P<0.01$  vs. Model group. DBD, 3,4-Dihydroxybenzaldehyde; UDP-GlcNAc, uridine diphosphate N-acetylglucosamine; OGT, O-GlcNAc transferase; MCAO/R, middle cerebral artery occlusion/reperfusion.

metabolic pathway by analyzing high-throughput metabolomic data and using multivariate statistical methods to elucidate its therapeutic mechanism. Initially, it was demonstrated that improving mitochondrial dysfunction attenuated brain I/R injury, which is consistent with previous studies (34,35). DBD could significantly reduce the neurological deficit and cerebral infarction volume in MCAO/R rats. In addition, neuronal loss caused by I/R can be reduced by inhibiting oxidative stress and mitochondrial damage. After determining the crucial role of mitochondria in cerebral I/R injury, the present study conducted follow-up studies using high-purity mitochondria extracted from rat ischemic lateral brain tissue. The experimental results showed that DBD improved mitochondrial dysfunction by enhancing the function of the neural mitochondrial respiratory chain, restoring the level of mPTP, reducing the loss of MMP and the transfer of mitochondrial Cyt-c to the cytoplasm, increasing the level of ATP and inhibiting apoptosis. However, mitochondria are not only the traditionally considered cellular engine but they also decompose nutrients through energy metabolism and divide metabolites to maintain redox homeostasis (36). Thus, mitochondria deserves our attention in terms of metabolic functions. The aforementioned studies have shown that DBD can effectively alleviate reperfusion injury in MCAO/R rats and that its effect is closely related to that of mitochondria. This result provides a reliable basis for our later metabolomic research.

The disturbance of energy metabolism is a significant cause of cerebral ischemia (37). Neuronal activity is closely associated with mitochondrial function (38). It was hypothesized that energy metabolism is primarily related to mitochondrial dysfunction and acts as a key target of cerebral I/R injury.

Further research on the mechanism by which DBD improves mitochondrial energy metabolism to maintain normal mitochondrial function and morphology is warranted to break the vicious circle following reperfusion injury. A number of studies have shown that cerebral I/R injury can peak within 24 h (27,35). Hence, metabolomics were used to reveal the neuroprotective effect of DBD and the metabolic pathways affected by DBD in cerebral I/R injury. The results showed that the metabolites involved in affected by DBD primarily included amino acids, nucleotides and their metabolites in brain tissue. DBD increased succinyl-CoA, UDP-GlcNAc, dTMP, AMP, UMP, IMP, fructose 1,6-bisphosphate and 6-Phosphogluconic acid, and especially UDP-GlcNAc. By contrast, DBD decreased the expression of PLA.

Pathways mediated by DBD were enriched for differential metabolites. The results highlighted fructose and mannose metabolism; tropane, piperidine and pyridine alkaloid biosynthesis; amino sugar and nucleotide sugar metabolism and pentose phosphate pathway (PPP). Glycolysis changes from aerobic to anaerobic pathway in cerebral ischemia because of ischemia and hypoxia and the PPP is activated as an endogenous antioxidant mechanism (39). 6-Phosphogluconic acid, the first metabolite of glycolysis and the initiator of PPP, works with glutathione peroxidase to eliminate excess ROS following stroke (40). Fructose 1,6-bisphosphate is a glycolytic intermediate that enhances glycolysis during hypoxia, preserves cellular ATP stores (41) and reduces oxidative stress (42). Similarly, activating the pathways of fructose and mannose metabolism can reduce oxidative damage in brain tissue, increase brain metabolism and play a neuroprotective role (43). The end product of glycolysis is pyruvate, which can enter the mitochondria to participate in

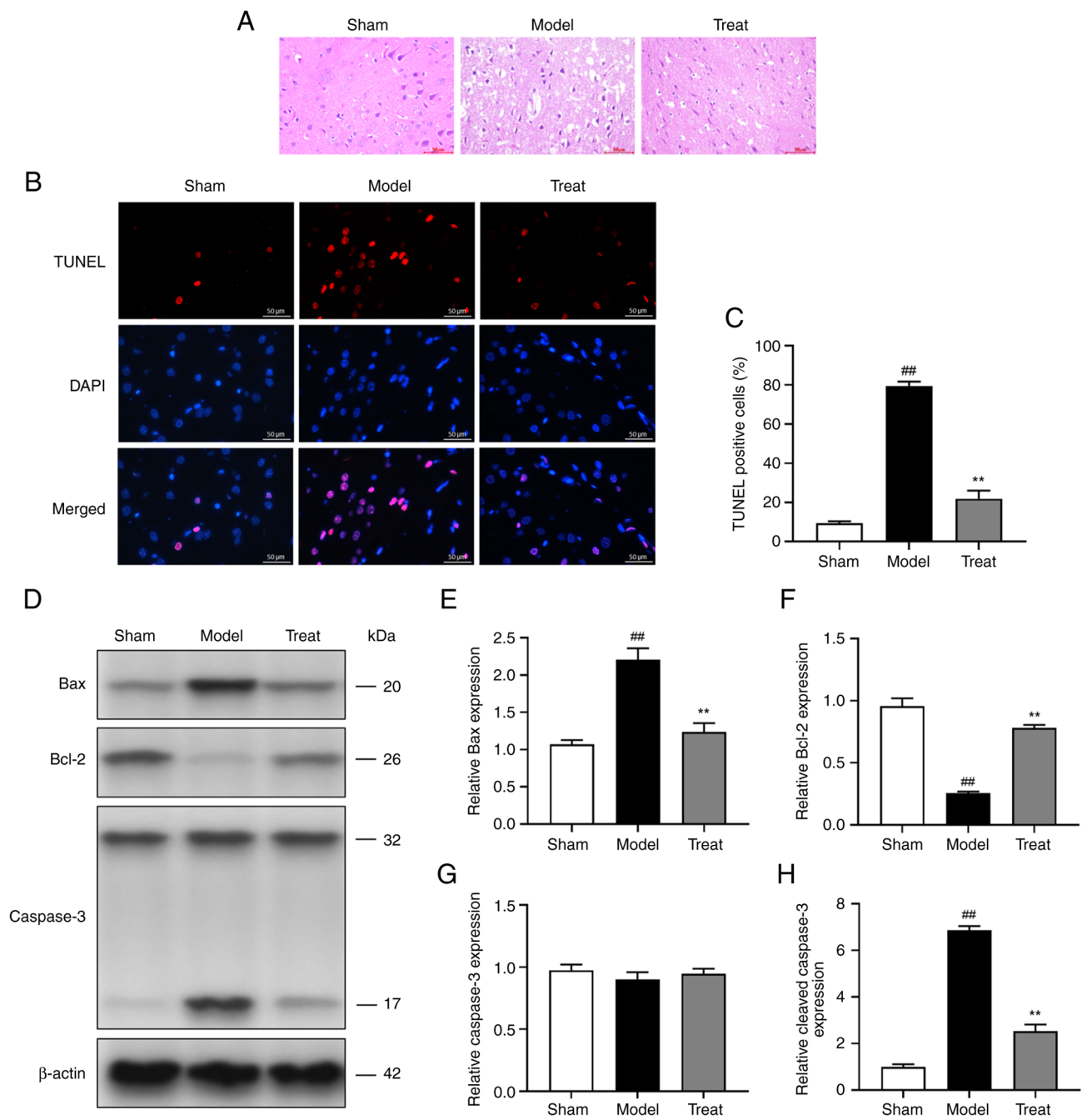


Figure 8. DBD attenuates MCAO/R-induced apoptosis in rat brain cells. (A) Hematoxylin and eosin staining of rat brain tissue. Note the cellular structure and arrangement of nerve fibers in brain tissue. (B) TUNEL (red) staining in TUNEL staining, nuclei were stained with DAPI (blue) and detected under a fluorescence microscope. (C) Quantitative analysis of apoptotic cells in brain tissue. (D) Representative western blot bands of apoptosis-related proteins are displayed. (E, F) Western blot analysis of Bax and Bcl-2 expression in brain tissue. (G and H) Western blot analysis of Caspase-3 and cleaved-Caspase-3 expression in brain tissue. All data are presented as the mean  $\pm$  standard error of the mean,  $n=3$ . Magnifications are  $\times 400$ ; scale bar= $50\ \mu\text{m}$  <sup>##</sup> $P<0.01$  vs. Sham group; <sup>\*\*</sup> $P<0.01$  vs. Model group. DBD, 3,4-Dihydroxybenzaldehyde; MCAO/R, middle cerebral artery occlusion/reperfusion; TUNEL, TdT-mediated dUTP nick end labeling.

the TAC cycle. Succinyl-CoA is a product of mitochondrial metabolism of propionyl-CoA, which is a component of the TAC cycle and it can participate in energy metabolism (44). Methylmalonyl-CoA, the major synthase of succinyl-CoA, affects stroke, dyskinesia and cognitive performance in the basal ganglia (45). Additionally, the PPP provides precursors for nucleotide and amino acid biosynthesis. Nucleotides and their metabolites are involved in basic life activities such as heredity, development and growth. Different bases, such as AMP, UMP, thymidine nucleotide (TMP) and IMP, have

become potential therapeutic targets for IS (46,47). In cells, impaired dTMP biosynthesis can lead to uracil misconjugation and accumulation of DNA strand breaks, inducing cell cycle arrest and apoptosis (48). Inosine can directly enter cells, convert into IMP to synthesize AMP and GMP, participate in ATP metabolism and then improve the activity of intracellular enzymes (49). Inosine can stimulate axonal regeneration *in vivo* after stroke, reduce neuronal apoptosis by downregulating the expression of Cyt-c and induce a protective effect against anti-cerebral I/R injury (50).

Among the aforementioned metabolites, DBD induces the most significant differential metabolite UDP-GlcNAc, which is a nucleotide sugar and the final product of the hexosamine biosynthesis pathway (HBP) in amino sugar and nucleotide sugar metabolism (51). UDP-GlcNAc provides a critical substrate for various biological processes, indirectly reflecting the nutritional status of cells and promoting neovascularization (50,52). Based on previous reports, increasing the amount of UDP-GlcNAc is a direct and effective method to correct the impaired activation of pro-survival pathways following ischemia in the aged brain (53). UDP-GlcNAc enables cell survival under various stresses and induces protective effect against brain I/R pressure by inhibiting mPTP opening and reducing neuronal apoptosis (54,55). Therefore, increasing UDP-GlcNAc to promote cell survival pathways may be a potential neuroprotective approach for treating stroke. In addition, based on the results of the present study, the expression of one metabolite (PLA) was downregulated. Experiments show that PLA interacts with rat brain mitochondrial hexokinase, which damages glucose metabolism in the brain and reduces ATP content (56). In addition, PLA has been shown to increase lipid peroxidation in rodent cerebral cortex and induce ROS and DNA damage in glial cells (33). In the present study, DBD ameliorated oxidative stress injury and energy metabolism disorders in brain mitochondria primarily by interfering with the aforementioned metabolic pathways and significantly different metabolites. This increased the production of ATP in the brain, inhibited neuronal apoptosis and reduced neuronal damage and brain cell death, which may be the metabolic mechanism through which DBD alleviates cerebral I/R injury.

It is also noteworthy that UDP-GlcNAc, a metabolite with a marked increase following DBD treatment, exhibited a neuroprotective effect. To determine the potential targets of DBD in the treatment of stroke, the content of UDP-GlcNAc in each metabolomics group was measured and it was found that DBD could significantly increase the level of UDP-GlcNAc. Therefore, it was hypothesized that DBD may inhibit brain cell death by increasing the level of UDP-GlcNAc. To confirm the mechanism by which UDP-GlcNAc increases DBD, the activity of OGT, a key metabolic enzyme of UDP-GlcNAc was confirmed. As UDP-GlcNAc is a direct donor substrate of OGT, its activity primarily reflects the intracellular concentration of UDP-GlcNAc. OGT is abundantly expressed in neurons, primarily in the nucleus and synapse and it plays a role in regulating neuronal process (57). OGT knockdown significantly reduces the translocation of dynamin-related protein 1 from the cytoplasm to mitochondria in the MCAO/R-induced mouse model of brain I/R injury and enhances mitochondrial fission, thereby leading to neuronal fission and increased apoptosis (58). Consistent with previous reports, the present study found that DBD could significantly increase the expression of OGT, indicating that DBD may increase the level of UDP-GlcNAc manifested as increased activity of OGT. In addition, OGT can be a therapeutic target for cerebral I/R.

Apoptosis is the final and significant determinant of I/R brain injury and inhibition of apoptosis is a crucial step in treating IS. Mitochondrial dysfunction is closely related to neuronal apoptosis during brain I/R injury (59). The present study examined the effect of DBD on mitochondrial apoptosis.

TUNEL staining can accurately reflect the most typical features of apoptosis. The experimental results showed that DBD can significantly reduce neuronal apoptosis. The HE staining of brain cells in the model group showed nuclear pyknosis and disordered arrangement of nerve fibers, whereas DBD could improve the pathological conditions of brain tissue. The ratio of anti-apoptotic proteins to pro-apoptotic proteins regulates cell survival. Bcl-2 is an anti-apoptotic protein that eliminates excess ROS generated during I/R (60). By contrast, Bax is a pro-apoptotic protein that causes MMP loss and Cyt-c release(6). Cyt-c is a crucial mitochondrial molecule (61); once released into the cytoplasm, it will induce the activation of the apoptotic enzyme activator and then activate the mitochondrial caspase apoptosis pathway to induce neuronal apoptosis (62). Similarly, the results of the present study suggested that DBD can effectively inhibit brain cell apoptosis and improve mitochondrial dysfunction by increasing UDP-GlcNAc, thereby alleviating I/R-induced neural damage. Additionally, apoptosis is inhibited with increased OGT expression, which may be an essential metabolic mechanism of DBD in treating IS.

In conclusion, the present study adopted a targeted energy metabolomic approach to explore the metabolite characteristics and underlying mechanisms associated with DBD treatment of cerebral I/R injury. Based on histopathological and metabolomic results, the present study confirmed the biological function of UDP-GlcNAc in DBD in the treatment of stroke. Notably, the regulatory enzyme OTC of UDP-GlcNAc is important for inhibiting I/R-induced neuronal apoptosis. However, the present study has certain limitations because of the complexity and variability of stroke pathogenesis. DBD was also found to be associated with a variety of differential metabolites and pathways, whereas other metabolites need further study. Of course, the present study still updates our understanding of the pathogenesis of brain I/R injury and the neuroprotective mechanism of DBD and provides a potential therapeutic target for stroke.

### Acknowledgments

Not applicable.

### Funding

This study was supported by the National Natural Science Foundation of China (grant no. 81960733) and the Xingdian Talent Support Program-Special for Young Talent (2022).

### Availability of data and materials

The datasets used and/or analyzed during the current study are available from the corresponding author on reasonable request.

### Authors' contributions

PC conceived the experiment, YL and XD participated in the experiments, LY analyzed the results, YL wrote the manuscript and prepared all graphics, and XD revised the manuscript. YL and XD confirm the authenticity of all the raw data. All authors read and approved the final manuscript.

## Ethics approval and consent to participate

All animal experiments were approved by the Animal Ethics Committee of Yunnan University of Traditional Chinese Medicine (Kunming, China; approval no. R-062021088).

## Patient consent for publication

Not applicable.

## Competing interests

The authors declare that they have no competing interests.

## References

- Feigin VL, Brainin M, Norrving B, Martins S, Sacco RL, Hacke W, Fisher M, Pandian J and Lindsay P: World stroke organization (WSO): Global stroke fact sheet 2022. *Int J Stroke* 17: 18-29, 2022.
- GBD 2019 Stroke Collaborators: Global, regional, and national burden of stroke and its risk factors, 1990-2019: A systematic analysis for the global burden of disease study 2019. *Lancet Neurol* 20: 795-820, 2021.
- Feigin VL, Roth GA, Naghavi M, Parmar P, Krishnamurthi R, Chugh S, Mensah GA, Norrving B, Shiue I, Ng M, *et al*: Global burden of stroke and risk factors in 188 countries, during 1990-2013: A systematic analysis for the global burden of disease study 2013. *Lancet Neurol* 15: 913-924, 2016.
- Lust WD, Taylor C, Pundik S, Selman WR and Ratcheson RA: Ischemic cell death: Dynamics of delayed secondary energy failure during reperfusion following focal ischemia. *Metab Brain Dis* 17: 113-121, 2002.
- Lim S, Kim TJ, Kim YJ, Kim C, Ko SB and Kim BS: Senolytic therapy for cerebral ischemia-reperfusion injury. *Int J Mol Sci* 22: 11967, 2021.
- Nhu NT, Li Q, Liu Y, Xu J, Xiao SY and Lee SD: Effects of mdv1-1 on neural mitochondrial dysfunction and mitochondria-mediated apoptosis in ischemia-reperfusion injury after stroke: A systematic review of preclinical studies. *Front Mol Neurosci* 14: 778569, 2021.
- Wu M, Gu X and Ma Z: Mitochondrial quality control in cerebral ischemia-reperfusion injury. *Mol Neurobiol* 58: 5253-5271, 2021.
- Hayashida K, Takegawa R, Shoaib M, Aoki T, Choudhary RC, Kuschner CE, Nishikimi M, Miyara SJ, Rolston DM, Guevara S, *et al*: Mitochondrial transplantation therapy for ischemia reperfusion injury: A systematic review of animal and human studies. *J Transl Med* 19: 214, 2021.
- Ma Z, Xin Z, Di W, Yan X, Li X, Reiter RJ and Yang Y: Melatonin and mitochondrial function during ischemia/reperfusion injury. *Cell Mol Life Sci* 74: 3989-3998, 2017.
- Vongsfak J, Pratchayasakul W, Apajai N, Vaniyapong T, Chattipakorn N and Chattipakorn SC: The alterations in mitochondrial dynamics following cerebral ischemia/reperfusion injury. *Antioxidants (Basel)* 10: 1384, 2021.
- Paul S and Candelario-Jalil E: Emerging neuroprotective strategies for the treatment of ischemic stroke: An overview of clinical and preclinical studies. *Exp Neurol* 335: 113518, 2021.
- Zhu T, Wang L, Feng Y, Sun G and Sun X: Classical Active ingredients and extracts of chinese herbal medicines: Pharmacokinetics, pharmacodynamics, and molecular mechanisms for ischemic stroke. *Oxid Med Cell Longev* 2021: 8868941, 2021.
- Zhu H, Liu C, Hou J, Long H, Wang B, Guo D, Lei M and Wu W: *Gastrodia elata* blume polysaccharides: A review of their acquisition, analysis, modification, and pharmacological activities. *Molecules* 24: 2436, 2019.
- Lin LC, Chen YF, Tsai TR and Tsai TH: Analysis of brain distribution and biliary excretion of a nutrient supplement, gastrodin, in rat. *Anal Chim Acta* 590: 173-179, 2007.
- Guo C, Wang S, Duan J, Jia N, Zhu Y, Ding Y, Guan Y, Wei G, Yin Y, Xi M and Wen A: Protocatechualdehyde protects against cerebral ischemia-reperfusion-induced oxidative injury via protein kinase cepsilon/Nrf2/HO-1 pathway. *Mol Neurobiol* 54: 833-845, 2017.
- Guo Y, Yang JH, He Y, Zhou HF, Wang Y, Ding ZS, Jin B and Wan HT: Protocatechuic aldehyde prevents ischemic injury by attenuating brain microvascular endothelial cell pyroptosis via lncRNA Xist. *Phytomedicine* 94: 153849, 2022.
- Li X, Xiang B, Shen T, Xiao C, Dai R, He F and Lin Q: Anti-neuroinflammatory effect of 3,4-dihydroxybenzaldehyde in ischemic stroke. *Int Immunopharmacol* 82: 106353, 2020.
- He F, Duan X, Dai R, Wang W, Yang C and Lin Q: Protective effects of ethyl acetate extraction from *Gastrodia elata* blume on blood-brain barrier in focal cerebral ischemia reperfusion. *Afr J Tradit Complement Altern Med* 13: 199-209, 2016.
- Feng J, Xu YL, Meng QT, Yan HW and He FY: Protective effect of protocatechuic aldehyde on neurovascular unit homeostasis damage in rats after cerebral ischemia-reperfusion injury. *China Pharmacy* 32: 1811-1817, 2021.
- Duan X, Wang W, Liu X, Yan H, Dai R and Lin Q: Neuroprotective effect of ethyl acetate extract from *Gastrodia elata* against transient focal cerebral ischemia in rats induced by middle cerebral artery occlusion. *J Tradit Chin Med* 35: 671-678, 2015.
- Zeng M, Shao C, Zhou H, He Y, Li W, Zeng J, Zhao X, Yang J and Wan H: Protocatechualdehyde improves mitochondrial energy metabolism through the HIF1alpha/PDK1 signaling pathway to mitigate ischemic stroke-elicited internal capsule injury. *J Ethnopharmacol* 277: 114232, 2021.
- Shah SH, Kraus WE and Newgard CB: Metabolomic profiling for the identification of novel biomarkers and mechanisms related to common cardiovascular diseases: Form and function. *Circulation* 126: 1110-1120, 2012.
- Medina S, Dominguez-Perles R, Gil JJ, Ferreres F and Gil-Izquierdo A: Metabolomics and the diagnosis of human diseases-a guide to the markers and pathophysiological pathways affected. *Curr Med Chem* 21: 823-848, 2014.
- Lu AP, Bian ZX and Chen KJ: Bridging the traditional Chinese medicine pattern classification and biomedical disease diagnosis with systems biology. *Chin J Integr Med* 18: 883-890, 2012.
- Beccaria M and Cabooter D: Current developments in LC-MS for pharmaceutical analysis. *Analyst* 145: 1129-1157, 2020.
- Cao G, Jiang N, Hu Y, Zhang Y, Wang G, Yin M, Ma X, Zhou K, Qi J, Yu B and Kou J: Ruscogenin attenuates cerebral ischemia-induced blood-brain barrier dysfunction by suppressing TXNIP/NLRP3 inflammasome activation and the MAPK pathway. *Int J Mol Sci* 17: 1418, 2016.
- Li J, Yu W, Li XT, Qi SH and Li B: The effects of propofol on mitochondrial dysfunction following focal cerebral ischemia-reperfusion in rats. *Neuropharmacology* 77: 358-368, 2014.
- Chong J and Xia J: MetaboAnalystR: An R package for flexible and reproducible analysis of metabolomics data. *Bioinformatics* 34: 4313-4314, 2018.
- Liu Y, Xue X, Zhang H, Che X, Luo J, Wang P, Xu J, Xing Z, Yuan L, Liu Y, *et al*: Neuronal-targeted TFEB rescues dysfunction of the autophagy-lysosomal pathway and alleviates ischemic injury in permanent cerebral ischemia. *Autophagy* 15: 493-509, 2019.
- Rich PR and Marechal A: The mitochondrial respiratory chain. *Essays Biochem* 47: 1-23, 2010.
- Nolfi-Donagan D, Braganza A and Shiva S: Mitochondrial electron transport chain: Oxidative phosphorylation, oxidant production, and methods of measurement. *Redox Biol* 37: 101674, 2020.
- Geng X, Shen J, Li F, Yip J, Guan L, Rajah G, Peng C, DeGracia D and Ding Y: Phosphoenolpyruvate carboxykinase (PCK) in the brain gluconeogenic pathway contributes to oxidative and lactic injury after stroke. *Mol Neurobiol* 58: 2309-2321, 2021.
- Faverzani JL, Steinmetz A, Deon M, Marchetti DP, Guerreiro G, Sitta A, de Moura Coelho D, Lopes FF, Nascimento LVM, Steffens L, *et al*: L-carnitine protects DNA oxidative damage induced by phenylalanine and its keto acid derivatives in neural cells: A possible pathomechanism and adjuvant therapy for brain injury in phenylketonuria. *Metab Brain Dis* 36: 1957-1968, 2021.
- Cheng H, Lv M, Mi R and Xue G: Amifostine ameliorates cerebral ischaemia-reperfusion injury via p38-mediated oxidative stress and mitochondrial dysfunction. *Folia Neuropathol* 58: 334-346, 2020.
- Li J, Ma X, Yu W, Lou Z, Mu D, Wang Y, Shen B and Qi S: Reperfusion promotes mitochondrial dysfunction following focal cerebral ischemia in rats. *PLoS One* 7: e46498, 2012.
- Spinelli JB and Haigis MC: The multifaceted contributions of mitochondria to cellular metabolism. *Nat Cell Biol* 20: 745-754, 2018.

37. Wang SD, Fu YY, Han XY, Yong ZJ, Li Q, Hu Z and Li ZG: Hyperbaric oxygen preconditioning protects against cerebral ischemia/reperfusion injury by inhibiting mitochondrial apoptosis and energy metabolism disturbance. *Neurochem Res* 46: 866-877, 2021.
38. Chen Y, Guo S, Tang Y, Mou C, Hu X, Shao F, Yan W and Wu Q: Mitochondrial fusion and fission in neuronal death induced by cerebral ischemia-reperfusion and its clinical application: A mini-review. *Med Sci Monit* 26: e928651, 2020.
39. Shin TH, Lee DY, Basith S, Manavalan B, Paik MJ, Rybinnik I, Mouradian MM, Ahn JH and Lee G: Metabolome changes in cerebral ischemia. *Cells* 9: 1630, 2020.
40. Imahori T, Hosoda K, Nakai T, Yamamoto Y, Irino Y, Shinohara M, Sato N, Sasayama T, Tanaka K, Nagashima H, *et al*: Combined metabolic and transcriptional profiling identifies pentose phosphate pathway activation by HSP27 phosphorylation during cerebral ischemia. *Neuroscience* 349: 1-16, 2017.
41. Espanol MT, Litt L, Hasegawa K, Chang LH, Macdonald JM, Gregory G, James TL and Chan PH: Fructose-1,6-bisphosphate preserves adenosine triphosphate but not intracellular pH during hypoxia in respiring neonatal rat brain slices. *Anesthesiology* 88: 461-472, 1998.
42. Park JY, Kim EJ, Kwon KJ, Jung YS, Moon CH, Lee SH and Baik EJ: Neuroprotection by fructose-1,6-bisphosphate involves ROS alterations via p38 MAPK/ERK. *Brain Res* 1026: 295-301, 2004.
43. Salau VF, Erukainure OL, Koorbanally NA and Islam MS: Catechol protects against iron-mediated oxidative brain injury by restoring antioxidative metabolic pathways; and modulation of purinergic and cholinergic enzymes activities. *J Pharm Pharmacol* 72: 1787-1797, 2020.
44. Dobson CM, Gradinger A, Longo N, Wu X, Leclerc D, Lerner-Ellis J, Lemieux M, Belair C, Watkins D, Rosenblatt DS and Gravel RA: Homozygous nonsense mutation in the MCEE gene and siRNA suppression of methylmalonyl-CoA epimerase expression: A novel cause of mild methylmalonic aciduria. *Mol Genet Metab* 88: 327-333, 2006.
45. Andreasson M, Zetterstrom RH, von Döbeln U, Wedell A and Svenningsson P: MCEE mutations in an adult patient with Parkinson's disease, dementia, stroke and elevated levels of methylmalonic acid. *Int J Mol Sci* 20: 2631, 2019.
46. Tanaka T, Ogita A, Usuki Y and Fujita K: Selective inhibition of embryonic development in starfish by long-chain alkyl derivatives of UMP, TMP and AMP. *Nat Prod Res* 23: 1572-1578, 2009.
47. Frenguelli BG and Dale N: Purines: From diagnostic biomarkers to therapeutic agents in brain injury. *Neurosci Bull* 36: 1315-1326, 2020.
48. Chon J, Stover PJ and Field MS: Targeting nuclear thymidylate biosynthesis. *Mol Aspects Med* 53: 48-56, 2017.
49. Moritz CE, Teixeira BC, Rockenbach L, Reischak-Oliveira A, Casali EA and Battastini AM: Altered extracellular ATP, ADP, and AMP hydrolysis in blood serum of sedentary individuals after an acute, aerobic, moderate exercise session. *Mol Cell Biochem* 426: 55-63, 2017.
50. Xu D, Ai Q, Chen X, Wang Z, Wei H, Zhou L, Mei Z and Ge J: Metabonomics study on naotaiyang extract alleviating neuronal apoptosis after cerebral ischemia-reperfusion injury. *Evid Based Complement Alternat Med* 2022: 2112433, 2022.
51. Murakami K, Kurotaki D, Kawase W, Soma S, Fukuchi Y, Kunimoto H, Yoshimi R, Koide S, Oshima M, Hishiki T, *et al*: OGT regulates hematopoietic stem cell maintenance via PINK1-dependent mitophagy. *Cell Rep* 34: 108579, 2021.
52. Wang ZV, Deng Y, Gao N, Pedrozo Z, Li DL, Morales CR, Criollo A, Luo X, Tan W, Jiang N, *et al*: Spliced X-box binding protein 1 couples the unfolded protein response to hexosamine biosynthetic pathway. *Cell* 156: 1179-1192, 2014.
53. Wang Z, Li X, Spasojevic I, Lu L, Shen Y, Qu X, Hoffmann U, Warner DS, Paschen W, Sheng H and Yang W: Increasing O-GlcNAcylation is neuroprotective in young and aged brains after ischemic stroke. *Exp Neurol* 339: 113646, 2021.
54. Jiang M, Yu S, Yu Z, Sheng H, Li Y, Liu S, Warner DS, Paschen W and Yang W: XBP1 (X-Box-Binding Protein-1)-dependent O-GlcNAcylation is neuroprotective in ischemic stroke in young mice and its impairment in aged mice is rescued by Thiamet-G. *Stroke* 48: 1646-1654, 2017.
55. Cheng J, Wu Y, Chen L, Li Y, Liu F, Shao J, Huang M, Fan M and Wu H: Loss of O-GlcNAc transferase in neural stem cells impairs corticogenesis. *Biochem Biophys Res Commun* 532: 541-547, 2020.
56. Ziamajidi N, Jamshidi S and Ehsani-Zonouz A: In-silico and in-vitro investigation on the phenylalanine metabolites' interactions with hexokinase of Rat's brain mitochondria. *J Bioenerg Biomembr* 49: 139-147, 2017.
57. Hart GW, Slawson C, Ramirez-Correa G and Lagerlof O: Cross talk between O-GlcNAcylation and phosphorylation: Roles in signaling, transcription, and chronic disease. *Annu Rev Biochem* 80: 825-858, 2011.
58. Zhao J, Dong L, Huo T, Cheng J, Li X, Huangfu X, Sun S, Wang H and Li L: O-GlcNAc transferase (OGT) protects cerebral neurons from death during ischemia/reperfusion (I/R) injury by modulating Drp1 in mice. *Neuromolecular Med* 24: 299-310, 2021.
59. He Z, Ning N, Zhou Q, Khoshnam SE and Farzaneh M: Mitochondria as a therapeutic target for ischemic stroke. *Free Radic Biol Med* 146: 45-58, 2020.
60. Pan Y, Wang N, Xia P, Wang E, Guo Q and Ye Z: Inhibition of Rac1 ameliorates neuronal oxidative stress damage via reducing Bcl-2/Rac1 complex formation in mitochondria through PI3K/Akt/mTOR pathway. *Exp Neurol* 300: 149-166, 2018.
61. Bajwa E, Pointer CB and Klegeris A: The role of mitochondrial damage-associated molecular patterns in chronic neuroinflammation. *Mediators Inflamm* 2019: 4050796, 2019.
62. Lai Y, Lin P, Chen M, Zhang Y, Chen J, Zheng M, Liu J, Du H, Chen R, Pan X, *et al*: Restoration of L-OPA1 alleviates acute ischemic stroke injury in rats via inhibiting neuronal apoptosis and preserving mitochondrial function. *Redox Biol* 34: 101503, 2020.



This work is licensed under a Creative Commons Attribution-NonCommercial-NoDerivatives 4.0 International (CC BY-NC-ND 4.0) License.